Transaction A: Civil Engineering
Vol. 16, No. 3, pp. 199–215

SCIENTIA
IRANICA

Shaking Table Test of a 1:2.35 Scale 4-Story Building Constructed with a 3D Panel System

O. Rezaifar[1], M.Z. Kabir[2,*] and A. Bakhshi[3]

Abstract. *The seismic behaviour of a 4-story building is investigated under horizontal excitation of simulated earthquakes. The model has been constructed with a 3D sandwich panel system without any conventional frame system in four storeys on a shaking table. The building has been modelled before construction. Due to the table limit, the scale factor of the model is chosen as 1:2.35 of a prototype. The shaking table test of the scaled model of the building is carried out under several ground motions to verify the safety of the system. The simulated motions were applied to the model in two-perpendicular directions, simultaneously. The failure mechanism and dynamic behaviour of the model, as a 3D-panel building, is investigated in this study. Also, the objective of the study is to obtain the seismic performances of the described structural system under dynamic loading such as linear and non-linear structural characteristics, hysteretic behaviour, deformability and failure mechanism. Using these shaking tests, structural responses such as seismic capacity and damage mechanics, the distribution of seismic forces and weak points in the structures are evaluated. In addition, the lateral deformations, e.g. storey drifts are measured experimentally in the time domain. Accelerometers are mounted to measure accelerations in both vertical and horizontal directions. The results indicate that the 3D-panel system, due to its being well-confined and its integrity, can resist mainly in the linear domain and has an adequate load bearing potential against moderate-intense seismic excitation.*

Keywords: *Shaking table test; Sandwich panels; 3D wall system; Dynamic analysis; Shotcrete; Seismic exitation.*

INTRODUCTION

3-D wall panels are used in the construction of exterior and interior load-bearing and non-load-bearing walls and floors of buildings of all types of construction. This system consists of a welded wire space frame integrated with a polystyrene insulation core. The wall panel is placed in position and a Wythe of concrete is applied to both sides. Figure 1 shows the details of the panel at a scaled level. The wall panel receives its strength and rigidity from the diagonal cross wires welded to the welded-wire fabric on each side. This combination produces a truss behavior, which provides rigidity and shear terms for a full composite behavior [1]. Speed of construction, weight lightening and thermal insulation are the marked advantages of building with such an innovative system.

Salmon et al. present the results of a full-scale test of a prototype sandwich panel under transverse loading in a vertical position [1]. Nijhawan measured experimentally the interface shear forces [2]. Eiena et al. used the plastic composite diagonal elements for implementation on the sandwich panel as the shear connector for increasing the thermal insulation of this system [3]. The PCI published comprehensive reports on sandwich panels representing technical information. Einea et al. suggested the mathematical solution of semi-composite panels by developing differential equations, and compared the analytical solution with a numerical finite element analysis [4]. Bush and Stine studied the flexural performance of composite pre-cast sandwich panels with diagonal connectors [5]. Bush and Wu presented a mathematical solution and a finite element model for the bending analysis of pre-stressed sandwich panels with truss diagonal shear

1. *Department of Civil Engineering, Semnan University, Semnan, P.O. Box 35195-363, Iran.*
2. *Department of Civil and Environmental Engineering, Amirkabir University of Technology, Tehran, P.O. Box 15875-4413, Iran.*
3. *Department of Civil Engineering, Sharif University of Technology, Tehran, P.O. Box 11155-9517, Iran.*
*. *Corresponding author. E-mail: mzkabir@aut.ac.ir*

Received 21 May 2007; received in revised form 3 September 2008; accepted 11 November 2008

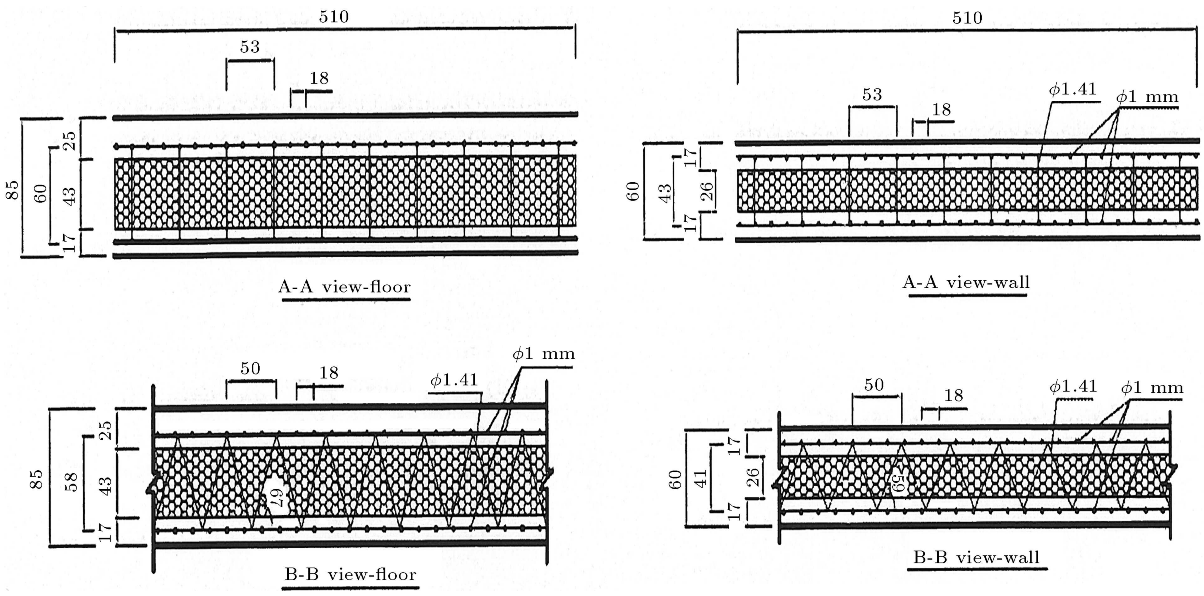

Figure 1. Model panel details (dimensions in mm).

members [6]. Nijhawan measured internal shear forces experimentally and designed shear connectors. Kabir and Hasheminasab in 2001, investigated the properties of 3D panels under flexural and shear loading on a 3D bearing wall and floor slab and showed its load-deflection curves and failure mechanism [7]. Benayoune et al. in an experimental investigation studied the ultimate strength behavior of Pre-cast Concrete Sandwich Panels (PCSP) under eccentric axial loading [8]. Deflection characteristics, variations of strains across the insulation layer, the strain in shear connectors, crack appearance and propagation under increasing load were recorded and analyzed in their work. In addition, in 2005, a comprehensive experimental research in order to better understand the mechanical characteristics of such a hybrid system was conducted by the first author [9]. The compressive strength of sprayed concrete in the form of small cores is measured as a factor of standard cylindrical specimens [10]. A shaking table test of 3D-wall panel systems in a six-storey scaled building was performed at the Tongji University in China [11].

The current work studies the dynamic behavior of load-bearing sandwich panels under earthquake motion. The mechanical properties of the members of a sandwich panel are obtained experimentally. The shear, flexural and compressive behavior of panel members has been investigated. Most studies on individual in-plane sandwich panels were studied statically. This study investigates the scaled four-storey sandwich panel building constructed on a shaking table. Some ground motions are applied progressively to the table and the dynamic structural responses of the building are measured.

SIMILITUDE RULE

An experimental scaled model must satisfy the necessary similitude requirements. Similitude requirements in static testing include physical, geometrical and boundary conditions. Besides these three requirements, the dynamic model should satisfy the following two requirements:

(a) The similitude of equilibrium equation of the point motion,

(b) The similitude of the original condition of the motion. [12]

The factor of strain similitude should equal one ($S_\varepsilon = 1$) while studying the nonlinear geometric and material problems or seismic and dynamic stability problems etc. All other requirements must be adjusted to satisfy certain relevant scale factors (Table 1). These requirements would represent a true-scale model in which all length quantities are scaled to geometric scale factor, S_L; materials with the same properties are used in the model and in the prototype ($S_E = 1$ and $S_\nu = 1$). The effective mass density of the model material must be artificially increased to the value of S_L. Non-dimensional material properties such as the Poisson ratio and the damping factor, also, have to be considered. Their values should be kept equal in the model and prototype if they have a significant effect on the response. Clearly, damping is influential in any dynamic problem requiring $S_\xi = 1$. This, again, calls for the use of the same basic materials in the model and prototype. Based on this Buckingham theory and because of construction restrictions and the limitation of the bearing weight of the shaking table, the scaling

Table 1. Scaling similitude rules.

Type	Physical Property	Similitude Relationship	Spec.
Material	Strain & poisson ratio	$S_\varepsilon = 1$ & $S_\nu = 1$	Control parameter in design
	Stress	$S_\sigma = S_E$	
	Modulus of elasticity	$S_E = 1$	
	Density	$S_\rho = S_\sigma / S_L$	
Geometric	Length & displacement	$S_L = S_L$ & $S_x = S_L$	
	Angle & area	$S_\beta = 1$ & $S_A = S_L^2$	
	Concentrate load & shear	$S_P = S_L^2$	
Load	Line load & surface load	$S_W = S_\sigma \times S_L$ & $S_q = S_\sigma$	
	Moment	$S_M = S_\sigma \times S_L^3$	
Dynamic	Mass	$S_m = S_\rho \times S_L^3$	S_m control parameter in design
	Stiffness	$S_K = S_E \times S_L$	
	Damping & damping ratio	$S_C = S_m/S_t$ & $S_\xi = S_C/\sqrt{S_K S_M}$	
	Time	$S_t = \sqrt{S_m/S_K} = \sqrt{S_L}$	S_a, S_g, S_t control parameter in dynamic loading
	Velocity	$S_\nu = S_x/S_t$	
	Acceleration and gravity	$S_a = S_x/S_t^2 = 1$ & $S_g = 1$	

factor has to be 2.35 ($S_L = 2.35$). According to this scaling, all dimensions in the prototype are scaled down by this factor. The modulus of elasticity of the model and density are E_m and $(\rho_0)_P + \rho_1$, respectively. By considering similitude relations, it is required that:

$$\left[\frac{g\ell(\rho_0+\rho_1)}{E}\right]_m = \left[\frac{g\ell\rho_0}{E}\right]_P. \tag{1}$$

So:

$$(\rho_0)_r + \frac{\rho_1}{(\rho_0)_P} = \frac{E_r}{\ell_r}, \tag{2}$$

$$(\rho_1) = \left[\frac{E_r}{\ell_r} - (\rho_0)_r\right](\rho_0)_P. \tag{3}$$

The simulation will be satisfied if the model's material density follows, using Equation 3. Therefore, additional mass should be applied to the model to obtain the exact dynamic response of the model. In this experiment, added masses were implemented at each floor to reach total model mass.

MATERIAL PROPERTIES

In order to verify accurate scaling and ensure that the system is working properly in accordance with the similitude law some component tests are defined. For the first step, the materials should behave correctly with the similitude law listed in Table 1. In this direction, the stress-strain curves should be the same as in the prototype and model material. Two major parts of the materials are steel and concrete. For the modeling of steel bars, the tension test is done and the stress-strain curve of the model is verified by the prototype. The maximum size of aggregates in concrete is 2.75 mm because of the scaling factor. The obtained average compressive stress, as displayed in Table 2 among several samples shows that $f'_c = 24.6$ MPa. Figure 1 shows the longitudinal and cross section of bearing 3D panels. The welded wire fabric of the model is considered with the cold rolling of a steel bar with a final outside diameter of 1.5 mm in accordance with ASTM A82, and an automated welding process in accordance with ASTM A185. The yield and ultimate strength of drawn and annealed wires are 470 and 680 MPa, respectively. The elongation of the mesh is 4.25%. Figure 2 shows the stress-strain curves for the welded wire fabric in the model and in the prototype. All specifications and details of materials are those experimentally measured and are addressed in Tables 3 and 4.

DESCRIPTION OF MODEL

Details of connections and the size and length of rebars are shown in Figure 3. The top view of the model on the shaking table with its connection and construction

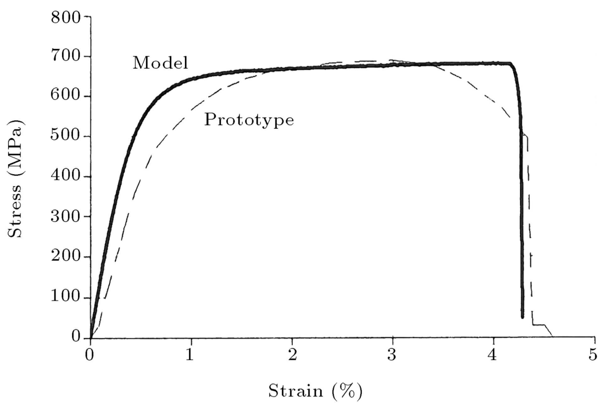

Figure 2. Stress-strain of model and prototype panel mesh wires.

Table 2. Concrete mix design sample.

Materials	Water (lit/m^3)	Cement (kg/m^3)	Sand (kg/m^3)	W/C
Density	260	500	1550	0.52

Table 3. Panel specification of the model (scaled specimen).

Panel Type	Thickness (mm)				Welded Wire Bar Size (mm)
	Total	Core	Upper Wythe	Bottom Wythe	
Wall Panel	60	25.5	17	17	1.5
Slab	85	42.6	25.5	17	1.5

Table 4. Material properties of test model.

Material	Poisson Ratio	Density kg/m^3	Young Modulus, GPa	Yield Stress, MPa	Tensile Strength, MPa	Compression Strength, MPa
Steel Bars	0.28	7855	206	470	-	-
Shotcrete	0.15	2175	15	-	2.8	24.6

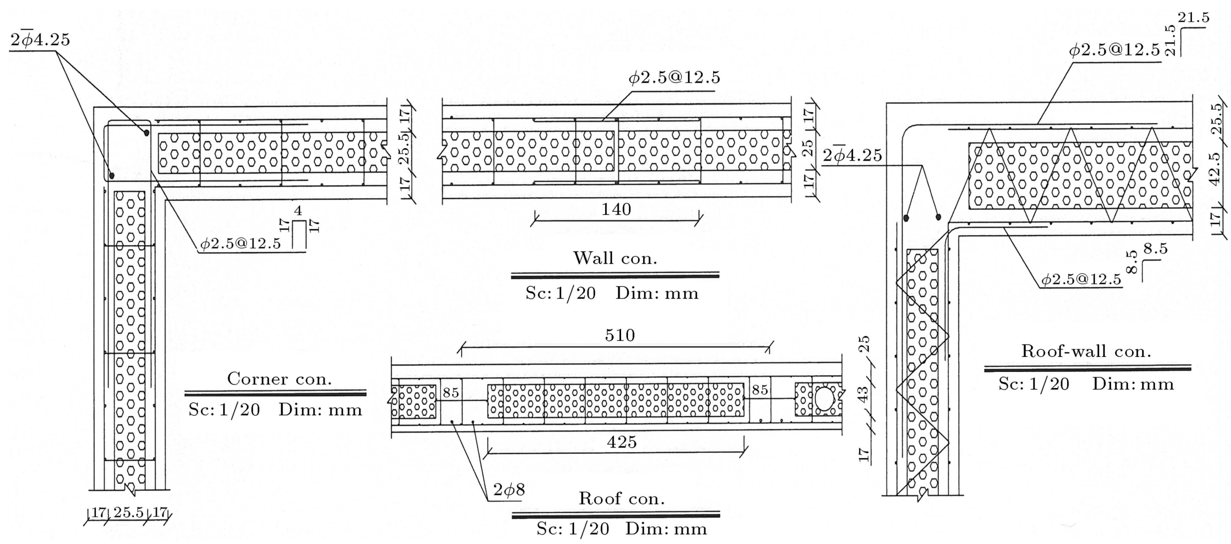

Figure 3. Connection details of panel in model style.

drawing of a four-story building based on scaled size is, respectively, shown in Figures 4 and 5. Also, Figure 6 shows some steps of the construction of the specimen. Wall and roof panels are installed in position and prepared for shotcrete. Panels and their additional reinforcement bars can be seen in this view of the specimen. Details of the roof and wall conjunction are observed from outside the building. Eight transducer sensors are used to measure displacements at each floor level in two directions. Sixteen accelerometer sensors are installed to measure the acceleration at each storey of a horizontal direction. For data correlation, three sensors are installed on the shaking table for measuring acceleration. Sixty-three sensors of strain gauges are installed on reinforced bars inside the model and connected to a data logger synchronized with a shaking motion. The strain gauge locations are shown in Figure 5. The exact locations of instruments are tabulated in Table 5. The measured displacements can show the effect of torsion, due to the accidental horizontal irregularity of the specimen during the applied record.

TEST PROGRAM

The dynamic loading applied on the specimen by the shaking table, starting from a set of diagnostic low level tests on the intact specimen, include white noise excitation and respective low-level to high level seismic excitations.

The base excitations records were applied to the building progressively. The original applied ground motion data is shown in Table 6. Acceleration time-histories of selected earthquakes are shown in Fig-

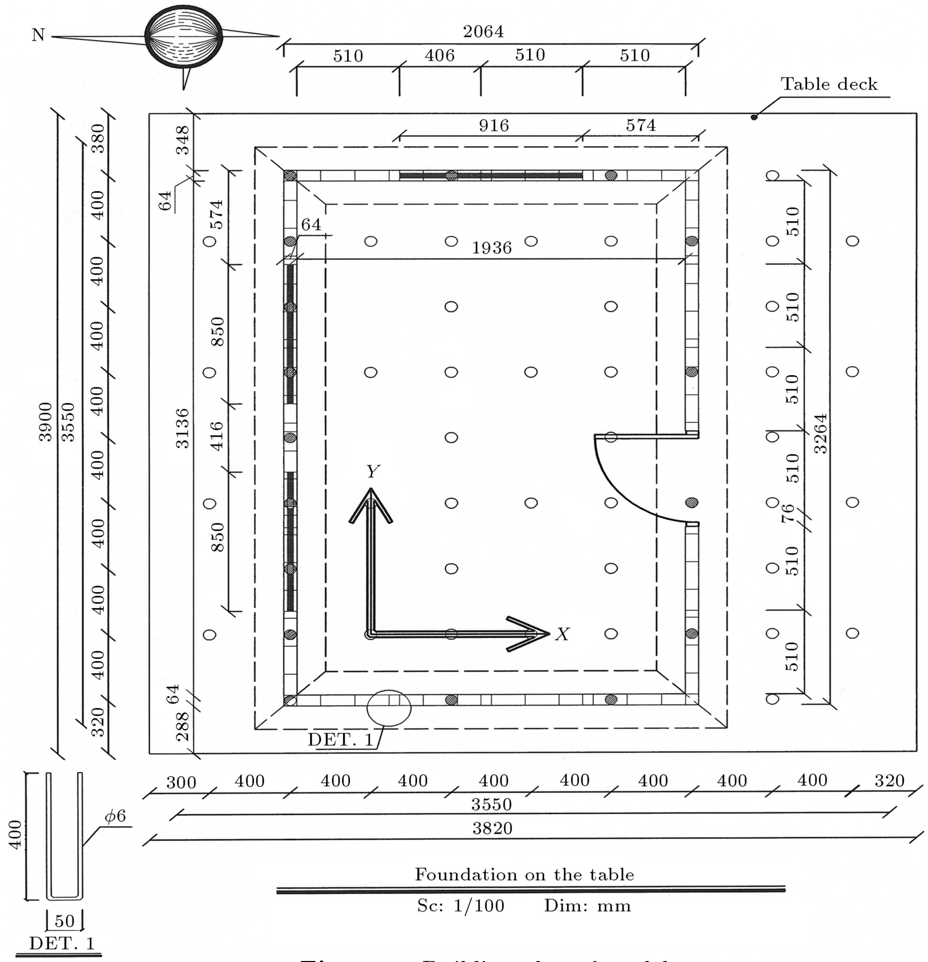

Figure 4. Building plan of model.

Table 5. Measurement points details and locations.

No.	Name	Type	Dir.	Level (m)	Location from Outside
1	ACC-1	Acceleration	Y	0	On the deck
2	ACC-2-3	Acceleration	X	0	On the deck
3	ACC-4-5-8-11-14	Acceleration	Y	0-1.30-2.60-3.80-5.00	Center of western wall
4	ACC-6-9-12-15	Acceleration	X	1.30-2.60-3.80-5.00	Left side of southern wall
5	ACC-7-10-13-16	Acceleration	X	1.30-2.60-3.80-5.00	Right side of southern wall
6	DIS-1-3-5-7	Displacement	Y	1.30-2.60-3.80-5.00	Center of western wall
7	DIS-2-4-6-8	Displacement	X	1.30-2.60-3.80-5.00	Left side of southern wall

Table 6. Applied ground motion records.

Name	Rec.	DUR (Sec.)	PGA-x (g)	PGV-x (mm/s)	PGD-x (mm)	PGA-y (g)	PGV-y (mm/s)	PGD-y (mm)
Elcentro-1940[§]	ELC	40.0	0.312	298.0	133.0	0.214	297.2	231.9
Naghan-1977[§§]	NGH	22.5	0.527	374.3	35.2	0.713	459.2	61.0
Northrige-1994[§§§]	NRT	40.0	0.990	776.2	304.5	1.779	1135.5	332.2

[§]: Imperial valley St., USA; [§§]: Zagros St., IRAN; [§§§]: Tarzana St., USA.

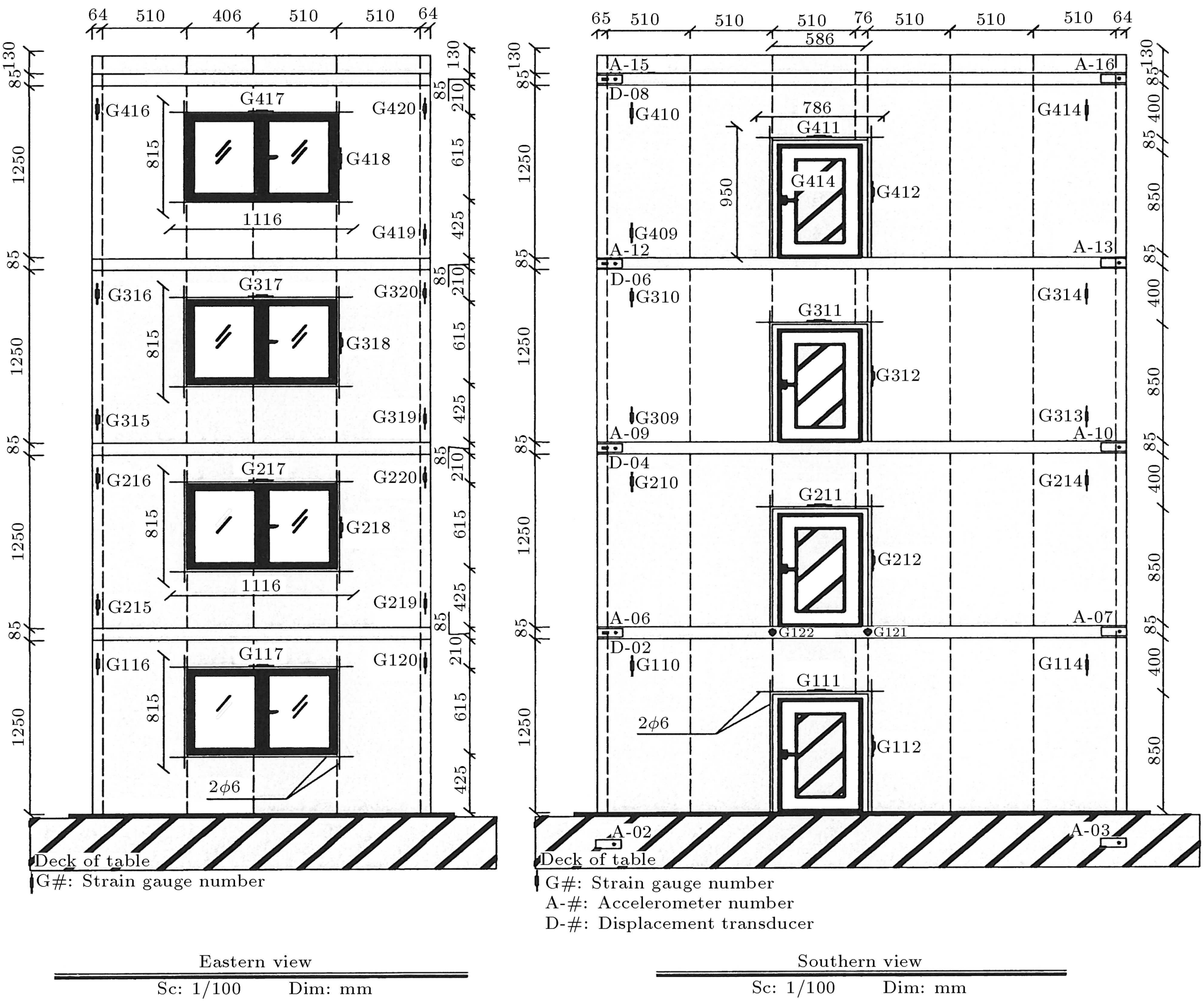

Figure 5. Model side views and the location of sensors.

Figure 6. Construction steps of the model.

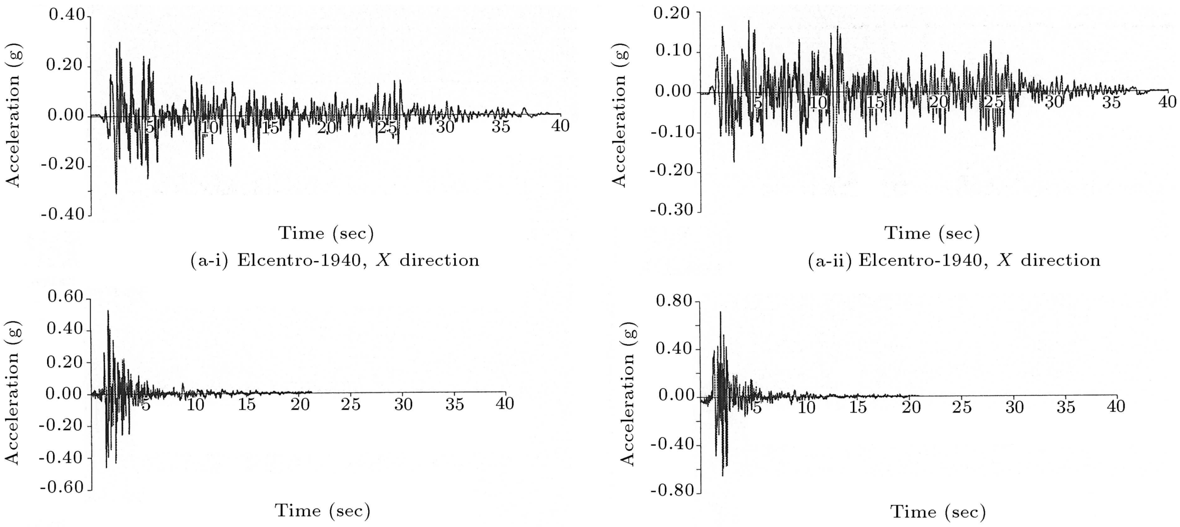

(a-i) Elcentro-1940, X direction

(a-ii) Elcentro-1940, X direction

(b-i) Naghan-1977, X direction

(b-ii) Naghan-1977, X direction

Figure 7. Selected applied ground motion records of acceleration in time history.

ures 7a and 7b. A summary of applied progressive ground acceleration is listed in Table 7. Tests were in both $E-W$ and $N-S$ directions, corresponding to progressively higher maximum input accelerations ranging from 0.1 g to 1.60 g. These tests are chosen for the analysis conducted in this paper. In order to recognize the frequency content of each record, using the Fast Fourier Transform Algorithm, the frequency content of each record component in an X and Y direction, is determined. The frequency content of the Elcentro record in X and Y directions is depicted in Figures 8a and 8b, respectively. In order to identify the primary natural period of applied records, the response spectra of Elcentro-1940 and Naghan-1977 are also calculated. Before and after the input of base motions, a white noise motion with a small level is applied to observe change in the natural frequency of the damaged model. The levels of table motion are determined based on preliminary analysis results and on consideration of obtaining the response data of the walls in the elastic domain, the near yield point and up to the ultimate state of the yield point or cracking. The description of shaking levels is presented in Table 7. It

Table 7. Applied ground motion records detail.

Level	**Symbol**	**PGA (g)**	**PGV (cm/s)**
	WN001		
A	AELC025	0.09	10.52
	WN002		
B	BELC100	0.38	42.09
	WN003		
C	CNGH135	1.20	79.98
	WN004		
D	DNRT080	1.63	110.04
	WN005		

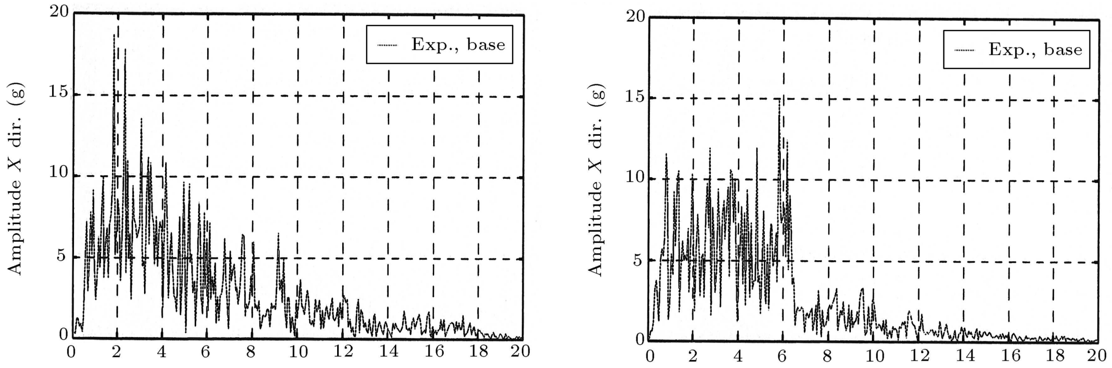

(a-i) Frequency content of Elcentro-1940, X direction

(a-ii) Frequency content of Elcentro-1940, Y direction

Figure 8. Applied motion records frequency content.

gives maximum accelerations and velocities obtained as horizontal maxima.

EXPERIMENTAL RESULTS AND DISCUSSION

Test Results of Specimen under Progressive Damage

Each state of damage inflicted by the strong motion excitations was followed by an inspection and careful documentation of the eventual cracks, which were marked on the concrete surface using different color markers, depending on the level of excitation. Next, these damages were drawn and documented. Figure 9 displays damage details and marked cracks. After each inspection of damage, low level, diagnostic excitations, as for the intact specimen, were carried out to investigate the changes during applied loads.

Based on progressive levels, the model is excited with the PGA ranging from 0.1 g to more than 1.6 g. In level A, the specimen completely behaves linearly and no cracks are observed in all wall areas. In level B, where the maximum acceleration reaches 0.3 g, some diagonal micro-cracks appeared around the first floor openings, indicating the stress concentration in this area. Additional reinforcing bars bear the tension forces in these positions. The cracks are formed only at the corners of the first storey openings. In the second and higher stories, almost no visual cracks have been observed. Vertical cracks along vertical ties appear under motions of about 1.0 g PGA. At the corners, U shaped reinforcement bars bear forces that are created by different deformations at the junction of perpendicular walls. There are also some flexural cracks caused by the disconnected walls around windows, in which the tensile forces are increased. Some uplift forces are exerted, due to the overturning action of the building and some cracks are made at the base levels. In level C, with the PGA above 1.0 g, larger cracks are seen at the wall areas around windows, especially on the first floor. However, cracks around the openings of upper stories are recognized, which reduce the structural stiffness of the system, but these are not severe in comparison with the first storey. The results teach that, in design considerations for the first storey, additional reinforcement is required with respect to higher-level details. Investigation of the frequency content of response motions clarifies that the model is sensitive to high-frequency records. Figure 9 shows the model after the test. The 2nd and 3rd stories of the building, after level E is shown in Figure 9b.

(a) Eastern wall

(b) Cracks in 2nd and 3rd level C

(c) Final cracks in west walls

(d) Final cracks in north walls

Figure 9. The model picture in duration of test level.

Figure 9c show the western wall after level E. It shows the flexural cracks in the critical line at a location between windows. Figure 9d shows the northern wall of the model in the first storey. The severe cracks at this location are induced by the unsymmetrical distributed stiffness of the building, and the torsion caused by ground motion produces such a failure mechanism. The allocation of vertical ties could help to absorb a part of the applied torsional energy. It shows that shear cracks in these sides are combined with corner diagonal cracks in the position of the windows. The cracks pass diagonally and lead to the vertical ties at the corner of the walls. The absence of such stiffened corner elements may cause a complete mechanism and lead to local collapse. Also, the wall between the north windows sustained extra shear because of its small length. In fact, this part of the wall behaves like a short column, which focused shears in this part. Diagonal cracks between windows in the north wall clarify the concentrated values of shear flow within it. It shows that similar wall parts need additional reinforcements.

System Frequency Content and Natural Period

Energy dissipation and the shear absorption capacity of structures are related to the dynamic characteristics of systems. One of them is natural frequency. It is a really challenging task to determine the natural frequencies of a sandwich panel system theoretically, due to its complicated composite behavior. The transfer function of the system shows the exact governing natural frequency of the system. In Figure 10, the plots of transfer functions of top acceleration, as obtained from accelerometers during the ELC025 test, are shown. As more and more cracks were appearing, the natural frequencies were getting lower and lower, in both directions. Transfer functions of accelerometers parallel to the Y-axis display the changes in the first natural frequency and torsional mode. The reduction of frequency of the first mode in the specimen during the test from level A to level D was observed. On the other hand, the transfer function obtained from the accelerometer parallel to the Y-axis shows changes of both the second mode along the Y-axis and the third torsional mode. In fact, the appeared modes in the transfer function of the Y direction include two major frequencies of the system. The first is because of translation modes in the Y direction, but the second is influenced by the torsional mode of the model. This is due to the lack of symmetry in stiffness with respect to the Y-axis and from the small coupling of the second mode with torsion.

The modal deformations and corresponding natural frequencies are obtained and listed in Table 8. A very good match can be observed both from the damaged specimen and from the intact model. However, some small coupling between the 2nd (along the x-axis) and the 3rd (torsional) modes is observed.

The initial natural frequencies of the system in X and Y directions are 8.11 Hz and 11.52 Hz, respectively. These components are unchanged during the base motion at level A. The natural frequency of the system is reduced by increasing ground PGA to more than 0.2 g. The natural frequencies of the system are about 3.30 and 5.49 Hz in X and Y directions after level B. The motions with an acceleration of 1.0 g maxima, level C, reduce the frequencies of the system down to 3.16 Hz and 4.32 Hz in X and Y directions, respectively.

The real values of prototype natural periods can be obtained by the similitude rules. Accordingly, the natural periods of the prototype are 0.18 seconds and 0.13 seconds in X and Y directions, respectively, which are obtained from the tested model. The approximate estimation of periods is as follows:

$$T = \alpha . H^{\frac{3}{4}}, \tag{4}$$

where T and H are the first natural period and the height of the building, respectively [13]. Factor α is calculated in experimental programs. For this system,

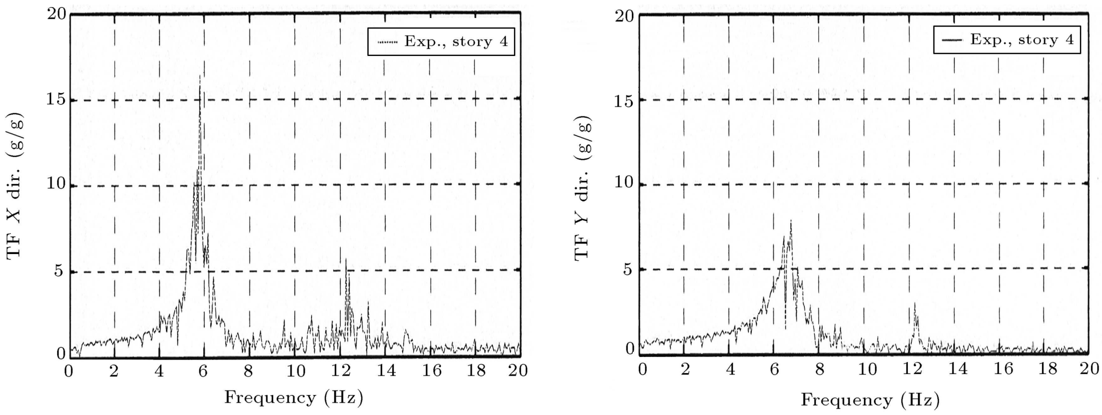

Figure 10. Transfer function of top accelerometers in ELC025.

Table 8. First natural frequency of the model in each level.

	Model-Frequency-Hz			Prototype-Period-s			Prototype-α	
	X	Y	R	X	Y	R	α_x	α_y
WN	8.11	11.52	15.00	0.18	0.13	0.10	0.027	0.019
A	5.89	6.53	8.03	0.25	0.23	0.19	0.037	0.033
B	5.31	3.97	5.31	0.28	0.38	0.28	0.041	0.055
WN	3.30	5.49	4.27	0.45	0.27	0.35	0.066	0.040
C	5.95	5.62	5.89	0.25	0.27	0.25	0.036	0.039
WN	3.16	4.32	7.75	0.47	0.35	0.19	0.069	0.050
D	6.60	13.55	6.84	0.23	0.11	0.22	0.033	0.016
WN	1.22	2.87	5.92	1.23	0.52	0.25	0.178	0.076

the calculated values (α) from the first row of Table 8, are 0.027 and 0.019 in X and Y directions, respectively. This factor is about 0.05 for traditional shear walls in codes. The differences between the new resulted values for α compared with RC frames and shear walls, show the high rigidity of the system. Furthermore, the low-flexibility steel used as welded wires in these systems (3D Panels) can lead to this high-frequency behavior. Degradation of rigidity in the duration of progressive PGA records made the system softer and it is seen that the system periods reach the RC frame after 1.0 g PGA records, because of substantial cracks at the first floor.

Structural Responses and Variation of Dynamic Amplification

The top acceleration responses are shown in Figure 11. The maximum value of the top response acceleration under the base motion of ELC025 is about 0.15 g in an X direction and 0.14 g in a Y direction. It can be seen from this figure that the system sustained the records successfully.

No major plasticity is occurred, because the displacement curves are fluctuated around the initial horizontal line. The maximum values of top displacement are about 12.94 mm and 22.27 mm in X and Y directions, respectively, under ELC025. The peak acceleration response is about 0.15 g and 0.14 g in X and Y directions, in the record. The peak value of input acceleration for ELC025 was about 0.05 g. The maximum of acceleration and displacement responses is presented in Tables 9 and 10.

The unidirectional simplified model of the specimen can be shown in Figure 12. For the undamped free vibration equation, the internal forces of the system will be obtained in Equation 5, and it can be written

Table 9. Maximum displacement response in ELC025 excitation (in mm).

	ELC025			
Story	$X+$	$X-$	$Y+$	$Y-$
4	8.73	12.94	8.26	22.77
3	8.71	12.93	8.22	22.69
2	8.53	12.87	8.19	22.61
1	8.43	12.82	8.15	22.5
Base	8.22	12.83	8.12	22.33

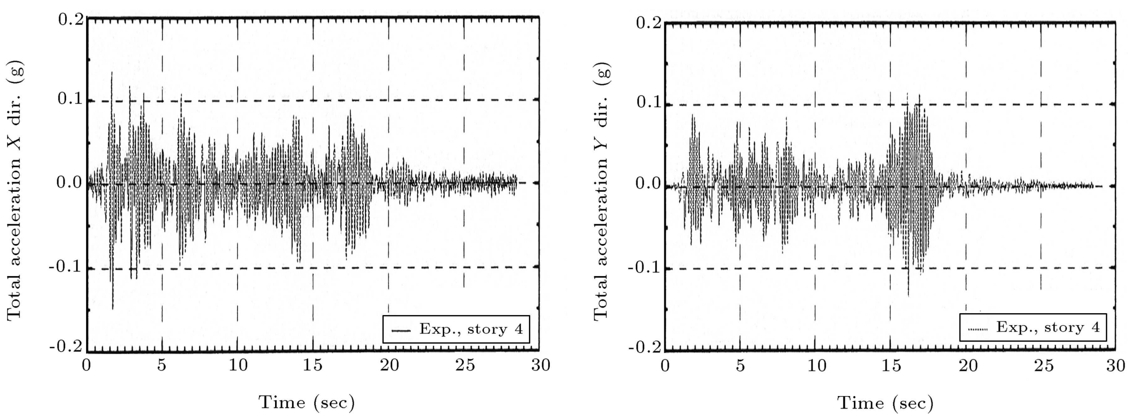

Figure 11. Top acceleration response of ELC025 in X and Y directions.

Table 10. Maximum acceleration response in ELC025 excitation (in g).

	ELC025			
Story	$X+$	$X-$	$Y+$	$Y-$
4	0.14	0.15	0.11	0.14
3	0.10	0.12	0.09	0.11
2	0.08	0.09	0.08	0.09
1	0.06	0.07	0.06	0.07
Base	0.07	0.05	0.05	0.04

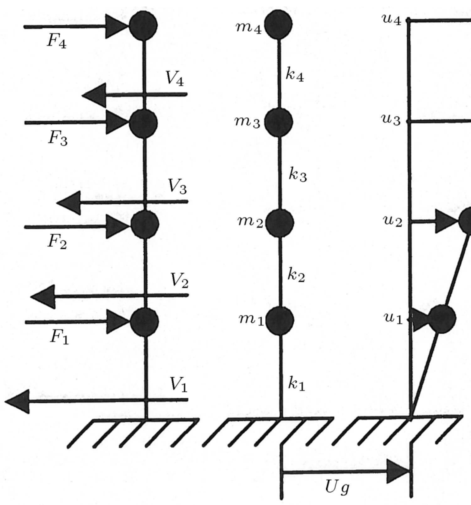

Figure 12. Storey shear at each level in unidirectional simplified model.

as Equation 6:

$$f_I + f_S = 0, \tag{5}$$

$$[M]\{\ddot{U}_t\} + [K]\{U\} = 0, \tag{6}$$

$$[M]\{\ddot{U}_t\} = \begin{bmatrix} m_1 & 0 & 0 & 0 \\ 0 & m_2 & 0 & 0 \\ 0 & 0 & m_3 & 0 \\ 0 & 0 & 0 & m_4 \end{bmatrix} \begin{Bmatrix} \ddot{u}_{t1} \\ \ddot{u}_{t2} \\ \ddot{u}_{t3} \\ \ddot{u}_{t4} \end{Bmatrix}$$

$$= \begin{Bmatrix} m_1.\ddot{u}_{t1} \\ m_2.\ddot{u}_{t2} \\ m_3.\ddot{u}_{t3} \\ m_4.\ddot{u}_{t4} \end{Bmatrix}, \tag{7}$$

$$[K]\{U\}$$

$$= \begin{bmatrix} k_1+k_2 & -k_2 & 0 & 0 \\ -k_2 & k_2+k_3 & -k_3 & 0 \\ 0 & -k_3 & k_3+k_4 & -k_4 \\ 0 & 0 & -k_4 & k_4 \end{bmatrix} \begin{Bmatrix} u_1 \\ u_2 \\ u_3 \\ u_4 \end{Bmatrix}. \tag{8}$$

A static relation leads to the following equation:

$$\begin{cases} F_4 = V_4 = k_4.(u_4 - u_3) = -m_4.\ddot{u}_{t4} \\ F_3 = V_3 - V_4 = k_3.(u_3 - u_2) - k_4.(u_4 - u_3) = -m_3.\ddot{u}_{t3} \\ F_2 = V_2 - V_3 = k_2.(u_2 - u_1) - k_3.(u_3 - u_2) = -m_2.\ddot{u}_{t2} \\ F_1 = V_1 - V_2 = k_1.(u_1) - k_2.(u_2 - u_1) = -m_1.\ddot{u}_{t1} \end{cases}$$

$$\rightarrow \begin{Bmatrix} F_1 \\ F_2 \\ F_3 \\ F_4 \end{Bmatrix} = - \begin{Bmatrix} m_1.\ddot{u}_{t1} \\ m_2.\ddot{u}_{t2} \\ m_3.\ddot{u}_{t3} \\ m_4.\ddot{u}_{t4} \end{Bmatrix}. \tag{9}$$

Static equivalent forces can be obtained from Equation 9, which are effected by each mass in the model. These values are equal to nodal forces. By considering Equation 6, forces of any mass can be find out as Equation 9. The stiffness value can be obtained and its numerical value for each excitation level is calculated by solving Equation 6.

The initial stiffness of the system is 21 kN/mm and 37 kN/mm in X and Y directions, respectively. The maximum reduction in stiffness value occurred at 0.5 g. The rate of change for the stiffness value is approximately similar in both X and Y directions, but it has a higher rate for the Y direction. The minimum values of stiffness are 2 kN/mm and 5 kN/mm in X and Y directions, respectively. This investigation shows that the system stiffness would decrease by 30% in an X direction and 16% in a Y direction without any visible damage. However, the system stiffness was decreased by 48% and 80% in X and Y directions, respectively, after 0.5 g PGA inputs. Finally, the stiffness of the system degraded down to 83% in the X direction and 82% in the Y direction, after 1.6 g PGA records were applied in X and Y directions, respectively, As plotted in Figure 13. The Y direction shows to be more stiffened than the X direction and this led to most nonlinearity in the variation of stiffness in the X direction.

The acceleration response of the model is introduced by an acceleration amplification parameter, A_{rms}, given by:

$$A_{rms} = \sqrt{\frac{1}{T} \int_0^{T_D} [a(t)]^2 dt},$$

$$B_{rms} = \frac{(A_{rms})_{\text{top}}}{(A_{rms})_{\text{bottom}}}, \tag{10}$$

where, A_r and A_g are the peak values of the acceleration responses of the structure and the acceleration input of the shaking table, respectively [14]. A_{rms} is the root mean square of acceleration of floor responses. The value of B_{rms} is calculated for each sensor

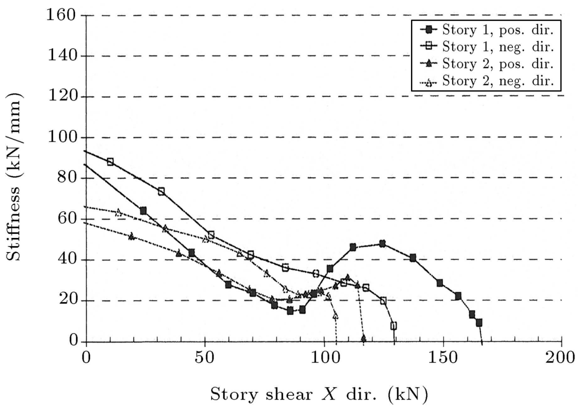

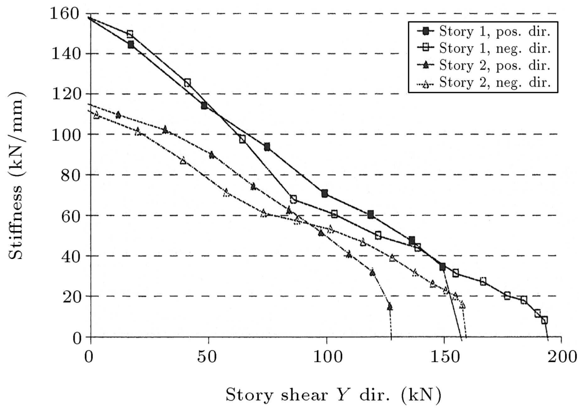

Figure 13. Stiffness degradation.

individually and the ratio of the measured value of top to bottom sensors shows the value of acceleration amplification. Usually, the value of B_{rms} increases with an increase of the structure rigidity. The tests showed that the value of B_{rms} at every measuring point decreased with an increase in seismic intensity.

The reason is that the stress–strain relationship of the model changed from linear to nonlinear because of micro-cracks, and the rigidity of the model decreased gradually. The variation of A_{rms} and B_{rms} values in both X and Y directions are plotted against the ground acceleration in Figure 14 and listed in Table 11. It is seen that, in the Y direction, up to 0.5 g the specimen

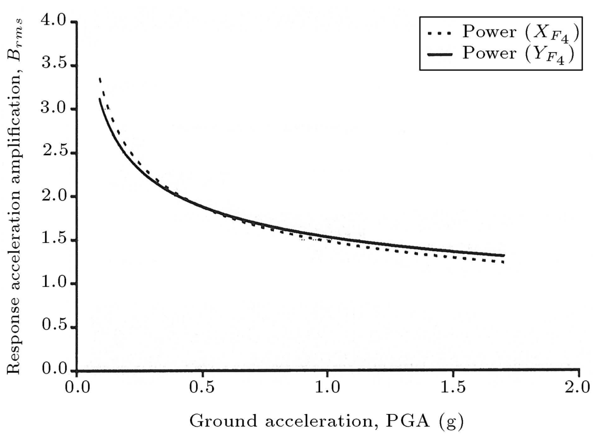

Figure 14. Response acceleration amplification.

behaves linearly and the value of B_{rms} sharply increases with a linear trend. The B_{rms} value then decays, due to a reduction in the response acceleration at the level of the crest, due to the appearance of some micro cracks in lower stories. This trend verifies the previous discussion regarding the commencement of the C level of applied earthquake intensity. However, the B_{rms} value in the X direction has a different trend compared to the Y direction. In fact, the response acceleration amplification of the X direction shows larger values with motions up to 0.5 g PGA, but it has a smaller value for motions bigger than 0.5 g PGA. The variation of B_{rms} indicates that the model has more stable behavior and an over-strength capacity, because of the longer length of walls in the direction, which caused a larger value of moment of inertia and shear resistance. This may be due to differences in the natural frequencies of the model in each direction and the frequency content of the input.

Storey Drifts, Storey Shear and Base Shear

The relative deformation of each storey is calculated by reciting the specified measuring points, as depicted in Figure 15, under ELC025 in a Y direction. Maximum relative storey drift is about 0.716 mm and the first storey drift of this direction is about 0.25 mm. The first and second storey values of displacement have different rates in height. The lateral deformation of

Table 11. Amplification factors of A_{rms} and B_{rms} in X and Y directions.

	ELC025				NGH135				NRT080			
Floors	A_{rmsX}	B_{rmsX}	A_{rmsY}	B_{rmsY}	A_{rmsX}	B_{rmsX}	A_{rmsY}	B_{rmsY}	A_{rmsX}	B_{rmsX}	A_{rmsY}	B_{rmsY}
4	0.048	3.00	0.039	2.79	0.124	1.63	0.162	1.60	0.234	1.49	0.258	1.52
3	0.038	2.38	0.034	2.43	0.098	1.29	0.130	1.29	0.180	1.15	0.210	1.24
2	0.030	1.88	0.027	1.93	0.086	1.13	0.112	1.11	0.162	1.03	0.171	1.01
1	0.023	1.44	0.020	1.43	0.086	1.13	0.109	1.08	0.175	1.11	0.162	0.95
base	0.016	1.00	0.014	1.00	0.076	1.00	0.101	1.00	0.157	1.00	0.170	1.00

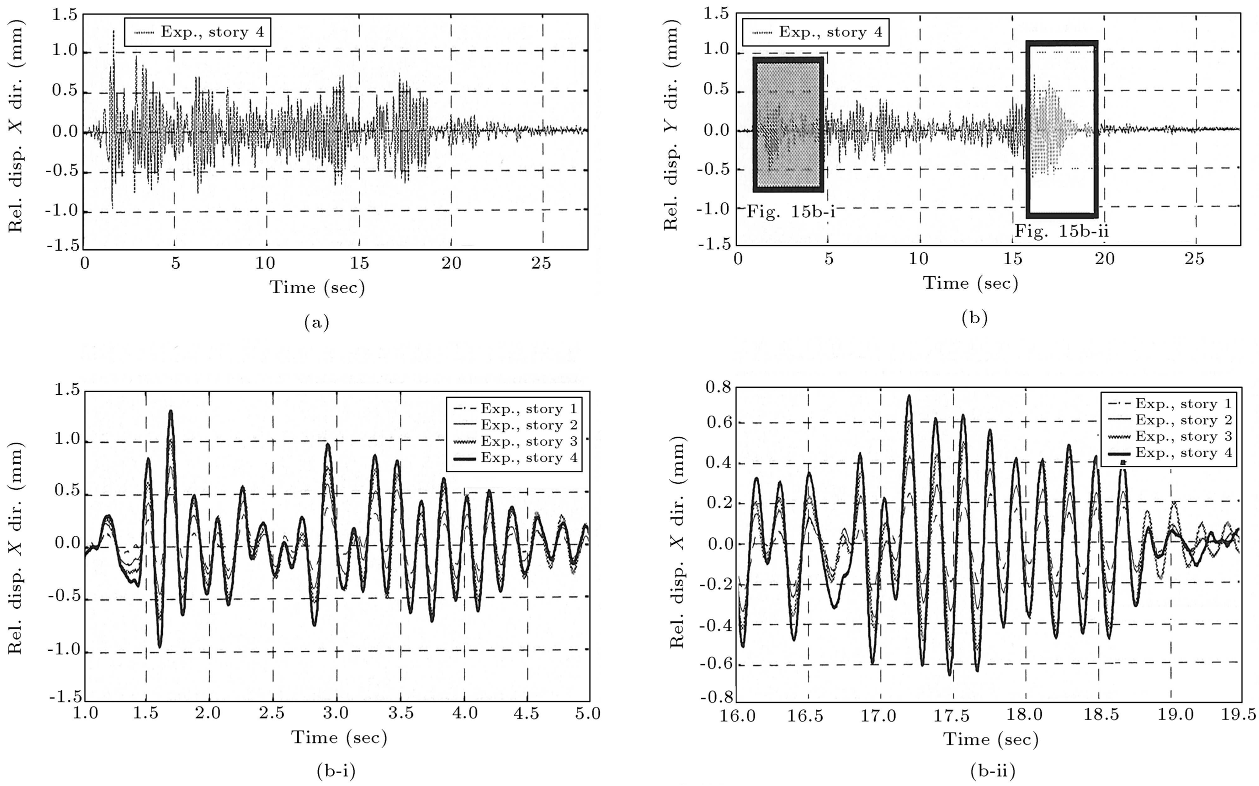

Figure 15. Relative displacement of stories in ELC025 record.

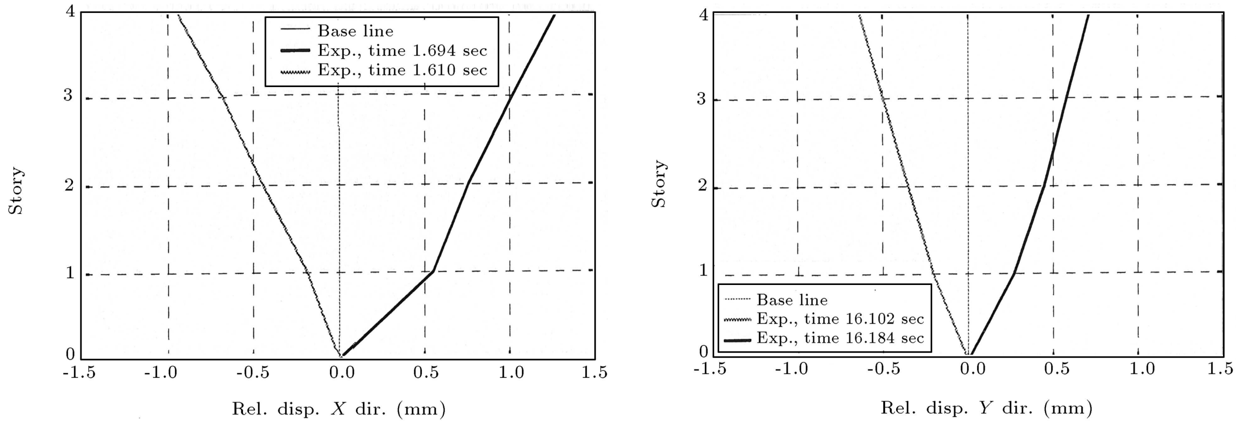

Figure 16. Relative peak displacement of stories at selected time in ELC025 excitation.

the system in the time of maximum response is plotted in Figure 16. By reference to this figure, the first mode deformation is distinguished brightly, which is because of the elastic behavior of the system. The system remains in the elastic region during the record. The lateral deformation of the system resulted in story drifts, shown in Figures 17 and 18. As can be seen, the system shows different rates of change in each direction and at each level. Because of more stiffness in the Y direction, the system behaves linearly in the direction rather than in the X direction. In fact, the lower stiffness of the X direction caused the first story to absorb the base shear more than the linear estimated values of stiffness in height. It shows that the effect of higher modes in the response, due to the natural properties of the system, is resulted from the special values of width/height. The bending stiffness in the X direction is lower than in the Y direction because of its width/height and width/length values. This fact makes the X direction affected by higher modes before the Y direction.

The storey shears of the system in height are presented in Table 12 and the shear profile is shown in Figure 19 for the selected tests. The storey shears of

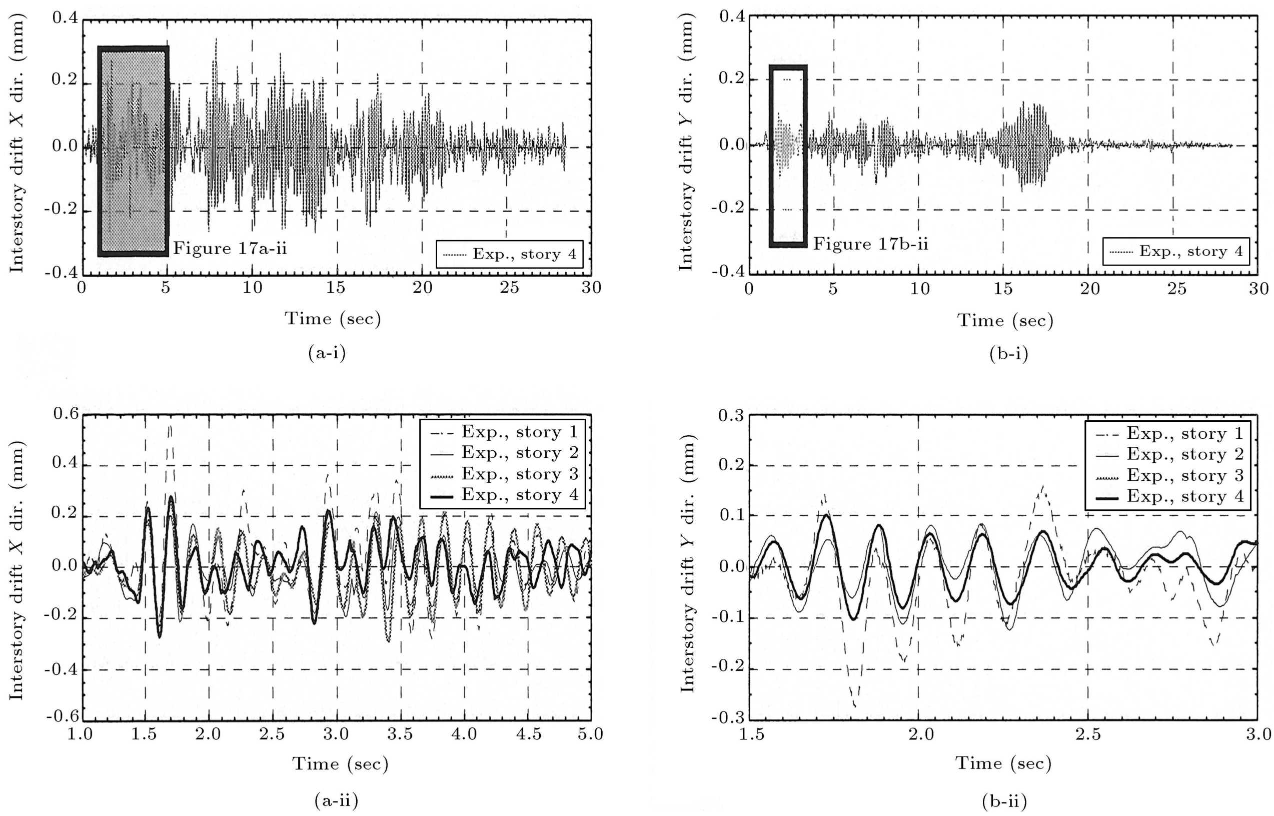

Figure 17. Storey drifts in ELC025 excitation.

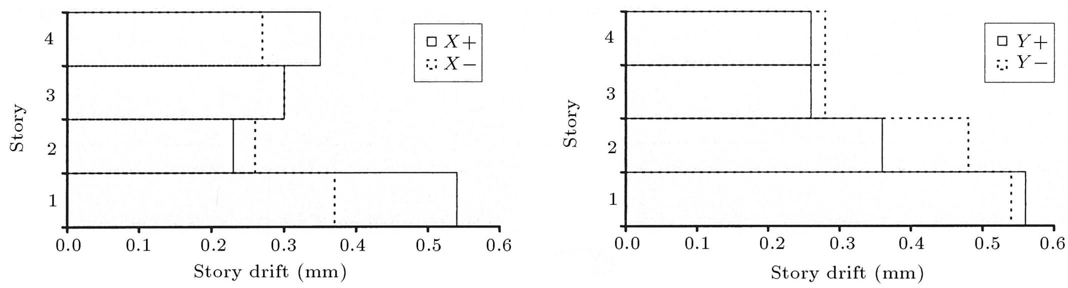

Figure 18. Storey drifts in ELC025 record at selected time.

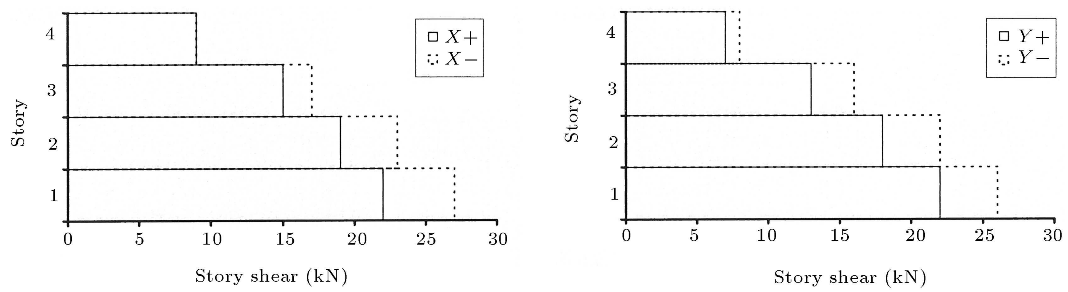

Figure 19. Storey shears in ELC025 excitation.

a Y direction have a rectangular distribution in height. In the regular frames, the base shear distribution form is a triangle and is rectangular for equipped frames. In the present system, the first storey absorbed more than 25 percent of the total shears. The maximum value of the base shear is about the value of weight of the model under records with 1.0 g PGA. It shows that the system has strongly rigid behavior due to its well-intensity. A different response in each direction shows the different capacity of the system in each direction.

Table 12. Storey shears in ELC025 and NGH135 (in kN).

	ELC025				NGH135			
	$X+$	$X-$	$Y+$	$Y-$	$X+$	$X-$	$Y+$	$Y-$
4	9	9	7	8	42	43	71	53
3	15	17	13	16	73	77	133	97
2	19	23	18	22	103	104	185	131
1	22	27	22	26	131	127	229	157

The Y direction is more stiffened and absorbed more than the X direction base shear; approximately equal to the weight of the model. In fact, the weight/base shear value is about 1.00 in the record of NGH135. It shows that the system behaves rigidly in the direction. Story shears in an X direction tend to a triangular distribution upward. The lateral loading of the X direction in positive direct has differences because of different arrangements of walls at each side of the directions. The rate of shears in the second, third and fourth floors is the same in elastic, ELC025, and inelastic, NGH135, records. However, it leads to some damage in the first floor in the inelastic region rather than in the elastic test. The time histories of story shears in X and Y directions are presented in Figure 20 for ELC025 and NGH135 excitations. Values are obtained after data correlation, which is verified, and the comparative frequency contents of each level force. The values of shears of each story contribution are different, because of the special content of records in each time. However, the overall contribution shows the same rate during the records.

Hysteresis Curves

Figure 21 shows the hysteresis curves of the model in X and Y directions under ELC025 records. Figures 21a and 21b show the base shear versus top deformation for ELC025 in X and Y directions, respectively. Figure 21a-ii shows the shear forces of the first storey versus its corresponding deformation under ELC025 records in an X direction. Comparing Figure 21a-i to 21a-ii, indicates that the first story dissipates about 50% of the total absorbed energy of the model. The model behaves quasi-linear up to 0.2 g PGA records. Nonlinearity is observed mostly over 0.50 g PGA. The hysteresis envelope curve could be pronounced in a stable manner demanding more capacity up to the failure mechanism. By references to hysteresis curves, the lower story absorbed energy more than the upper stories. Also, the Y direction is more stiffened than the X direction. Long walls with higher bending inertia and shear stiffness might be its cause. Figure 21c shows the nonlinear behavior of the model under the Naghan record that is scaled to 135 percent of the original. This figure shows that the system begins with nonlinear

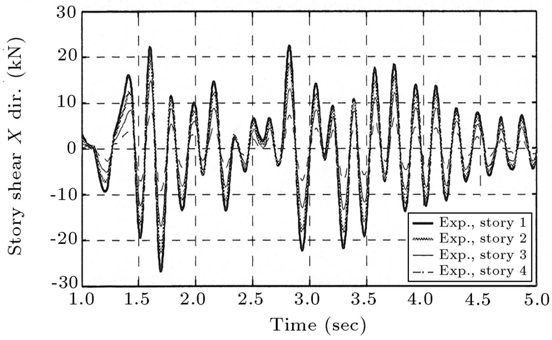

(a-ii) ELC025, Y direction

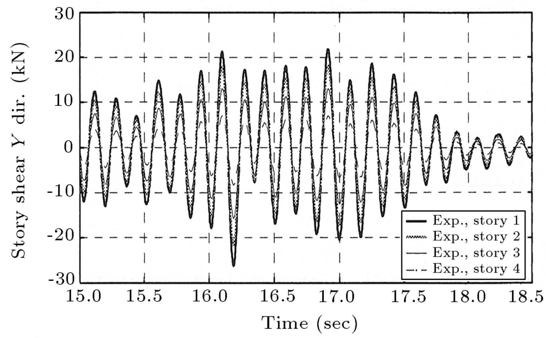

(a-i) ELC025, X direction

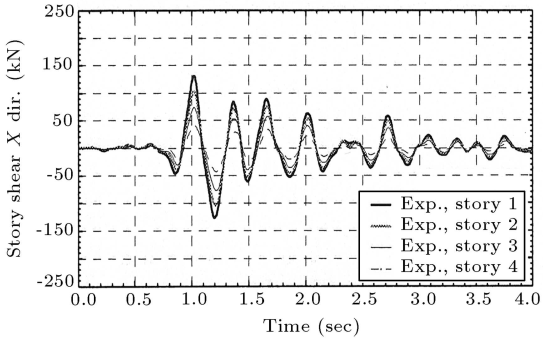

(a-ii) NGH135, Y direction

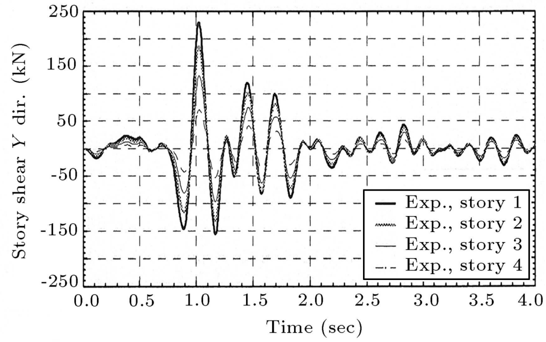

(a-i) NGH135, X direction

Figure 20. Storey shears under NGH135 excitation.

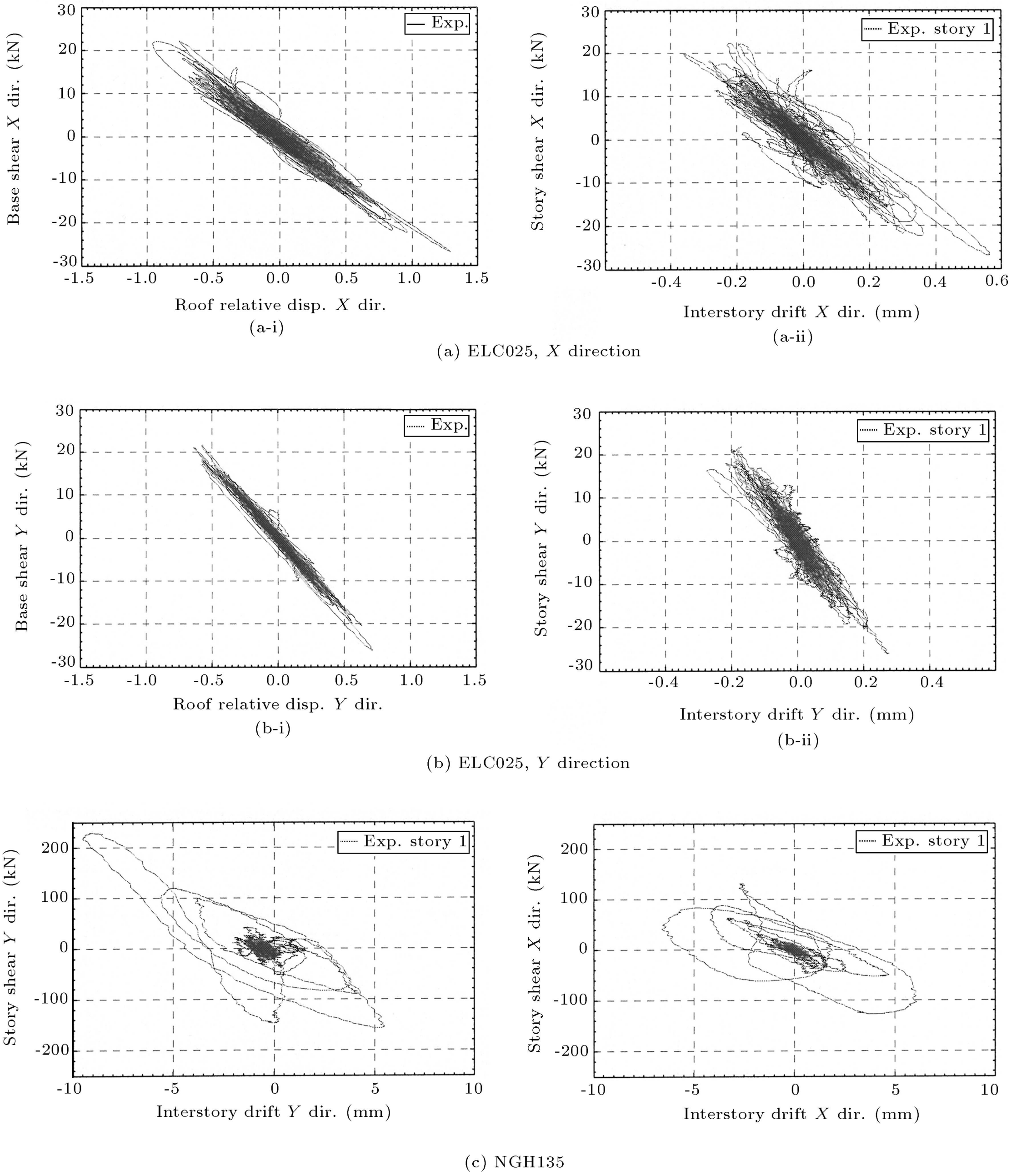

Figure 21. Hysteresis curves under excitations.

curves and hystersis curves get bigger loops and absorb more energy during recording.

CONCLUSION

In this investigation, a 1:2.35 scaled dynamic test of a four-storey building is carried out under several ground motions. The initial natural frequency of the system in an X direction is 8.11 Hz and 11.52 Hz in a Y direction. The natural frequency of the system is reduced by increasing acceleration. The model frequencies are declined down to 3.5 and 4.5 Hz in X and Y directions, respectively, when the model exercises ground acceleration up to 1 g. The storey shear distribution is approximately rectangular in the Y direction. The shear deformation in the X direction is downward, where the first storey contributes more than 25% of the base shear. In the presented system, the failure mechanism takes place at the first floor introduced by weak points at the opening locations in the form of diagonal cracks, showing the stress concentration in those locations and demanding additional reinforcing bars. However, in non-linear regions where the initial cracks appear, the system behaves with a relatively high behavior-factor, because of high over-strengthening, and the small columns provided at the corners help the building resist earthquakes by absorbing additional energy. The system has a certain life safety and good overall stability under high-intense earthquakes.

ACKNOWLEDGMENT

The authors gratefully acknowledge the financial support for providing, constructing and conducting the current tests by the Prefabricated SAP Company in Tehran. In addition, the contribution of the staff at the EERC, shaking table laboratory, Civil Eng. Dept. of Sharif University of Technology, is strongly acknowledged.

NOMENCLATURE

α	constant coefficient
$ACC\#\#$	acceleration measure point
A_g	peak value of the acceleration input
A_r	peak value of the acceleration response
C	damper matrices
$DIS\#\#$	displacement measure point
f	frequency of system
F	acceleration amplification factor
H	height of specimen
k	stiffness of system
K	stiffness matrices
K_x, K_y	stiffness in X and Y directions
m	mass of system
M	mass matrices
PGA	peak ground acceleration
PGD	peak ground displacement
PGV	peak ground velocity
R	exerted load vector
R_x, R_y	reaction of support (base shear) in X and Y directions
T	natural period of system
TF_x, TF_y	transfer function in X and Y directions
W/C	water to cement ratio
WWF	Welded Wire Fabricated,
#/#/#/#	Warp bar size/Woof bar size/ Warp Spacing/ Woof spacing
$\underset{\sim}{u}, \underset{\sim}{\dot{u}}, \underset{\sim}{\ddot{u}}$	displacement, velocity and acceleration vector

REFERENCES

1. Salmon, D.C., Eiena, A., Tadros, M.K. and Culp, T.D. "Full scale testing of precast concrete sandwich panels", *ACI Journal*, **94**, pp. 354-362 (1997).
2. Nijhawan, J.C. "Insulated wall panels interface shear transfer", *PCI Journal*, pp. 98-101 (1998).
3. Eiena, A., Tadros, M.K., Salmon, D.C. and Culp, T.D. "A new structurally and thermally efficient sandwich panel system", *PCI Journal*, **39**(4), pp. 90-101 (1994).
4. Einea, A., Salmon, D.C., Tadros, M.K. and Culp, T. "Partially composite sandwich panel deflection", *ASCE J. Struct. Eng.*, **12**(940), pp. 778-783 (1995).
5. Bush, T.D. and Stine, G.L. "Flexural behavior of composite precast concrete sandwich panels with continuous truss connectors", *PCI Journal*, **39**(2), pp. 112-121 (1994).
6. Bush, T.D. and Wu, Z. "Flexural analysis of prestressed concrete sandwich panels with truss connectors", *PCI Journal*, **43**(5), pp. 76-86 (1998).
7. Kabir, M.Z. and Hasheminasab, M. "Mechanical properties of 3D wall panels under shear and flexural loading", *CSCE Conference*, June 5-8, Montreal Canada (2002).
8. Benayoune, A., Aziz, A., Samad, A., Trikha, D.N., Abang Ali, A.A. and Ashrabov, A.A. "Structural behavior of eccentrically loaded precast sandwich panels", *Construction and Building Materials*, Elsevier, Article in press (2006).
9. Kabir, M.Z. "Structural performance of 3D sandwich panels under shear and flexural loading", *Scientia Iranica Journal*, **12**(4), pp. 402-408 (2005).
10. Kabir, M.Z. and Rahbar, M.R. "Experimental relation between non-destructive test and standard cylinder in shotcrete used in bearing 3D wall panels", *Third International Conference on Construction Materials*, Vancouver, Canada, August 22-24 (2005).
11. Weixing, S. and Lixin, Z. "Report of earthquake resistant test of the model of Evg-3d project, state laboratory for disaster reduction in civil engineering", *Shaking Table Testing Division of Tongji University* (Nov. 1997).
12. Harris, H.G. and Sabnis, G.M. "Structural modeling and experimental techniques", 2nd Edition, *ISBN* 0-8493-2469-6 (1999).
13. "Structural Engineers Association of California, *Uniform Building Code*, Whiter, Calif. (1997).
14. Wirsching, P.H., Paez, T.L. and Oritz, K., *Random Vibration: Theory and Practice*, John Wiley & Sons, Inc., New York (1995).